Measurements of the Coulomb dissociation cross section of 156 MeV ^{6}Li projectiles at extremely low relative fragment energies of astrophysical interest

J. Kiener,* H. J. Gils, H. Rebel, S. Zagromski, G. Gsottschneider, N. Heide, H. Jelitto, and J. Wentz
Kernforschungszentrum Karlsruhe, Institut für Kernphysik, P.O.B. 3640, D-7500 Karlsruhe, Germany

G. Baur
Forschungszentrum Jülich, Institut für Kernphysik, P.O.B. 1913, D-5170 Jülich, Germany
(Received 21 March 1991)

Coulomb dissociation of light nuclear projectiles in the electric field of heavy target nuclei has been experimentally investigated as an alternative access to radiative capture cross sections at low relative energies of the fragments, which are of astrophysical interest. As a pilot experiment the breakup of 156 MeV ^{6}Li projectiles at ^{208}Pb with small emission angles of the α particle and deuteron fragments has been studied. Both fragments were coincidentally detected in the focal plane of a magnetic spectrograph at several reaction angles well below the grazing angle and with relative angles between the fragments of 0°–2°. The experimental cross sections have been analyzed on the basis of the Coulomb breakup theory. The results for the resonant breakup give evidence for the strong dominance of the Coulomb dissociation mechanism and the absence of nuclear distortions, while the cross section for the nonresonant breakup follows theoretical predictions of the astrophysical S factor and extrapolations of corresponding radiative capture reaction cross section to very low c.m. energies of the α particle and deuteron. Various implications of the approach are discussed.

I. INTRODUCTION

Apart from the general interest in a basic understanding of nuclear reaction mechanisms, breakup processes of nuclear projectiles under the influence of the Coulomb field are of particular interest since they provide information on electromagnetically induced interactions of the projectile constituents [1,2]. The situation of pure Coulomb breakup can be experimentally approached by scattering at energies either below the Coulomb barrier or at higher energies, for collisions with small deflection angles and sufficiently large impact parameters beyond the range of the nuclear interaction. The situation for energies well above the Coulomb barrier has recently been scrutinized [3–5] in view of interesting possibilities of studying charged-particle reactions of astrophysical interest. The method and procedures proposed for extraction of astrophysical information are the subject of a current discussion [6,7].

The breakup may result either from transitions to free continuum states of the fragments or from transitions via resonance states above the breakup threshold followed by a subsequent disintegration into fragments. This (resonant) sequential breakup was found to be dominant at small relative energies of the particles (emitted in a narrow angular cone). The extent to which the *Coulomb* interaction governs this two-step mechanism at higher energies has not been extensively studied, though experimental observations of the $^6\mathrm{Li}\rightarrow\alpha+d$ [8–11] and $^7\mathrm{Li}\rightarrow\alpha+t$ [12–14] breakup in the field of heavy target nuclei indicate considerable contributions of Coulomb breakup to sequential processes via resonant states. The (nonresonant) direct Coulomb breakup appears to be a mode of interest in itself. While for sequential processes the lifetime of the resonances is much larger than the collision time, the direct breakup involves energy-dependent transition matrix elements into the continuum of the fragments distorted by the Coulomb field present at the breakup point. Though the analyses [12,15] of direct Coulomb breakup of ^{7}Li indicate that for energetic fragments with small relative energies a description as Coulomb excitation of quasibound states stays essentially correct, a conclusive investigation on the basis of adequate experimental data is still missing. The recent interest stems from the proposal [3–5] to use Coulomb breakup as an access to those nuclear transition matrix elements which determine the time-reversed process of Coulomb breakup, radiative capture reactions at astrophysical energies.

The present work addresses these questions by an experimental investigation of the breakup of 156 MeV ^{6}Li projectiles in the Coulomb field of ^{208}Pb nuclei. Alpha particle and deuteron fragments from elastic breakup, coincidently emitted in extreme forward direction with small relative energies, are observed in kinematically complete measurements with a dedicated detector setup using the magnetic spectrograph "Little John" [16] at the Karlsruhe Isochronous Cyclotron. The special interest in the case of ^{6}Li has several reasons.

(1) The production of Li isotopes through $^4\mathrm{He}(t,\gamma)^7\mathrm{Li}$ and $^4\mathrm{He}(d,\gamma)^6\mathrm{Li}$ fusion reactions at temperatures corresponding to energies of about 300 keV is an important clue of the nucleosynthesis in the primordial fire ball [17]. The $^4\mathrm{He}(d,\gamma)^6\mathrm{Li}$ cross section is unknown at these energies, and the present conclusion that ^{7}Li is produced in the big-bang nucleosynthesis, ^{6}Li, however, predominant-

ly by spallation reactions, is based on a purely theoretical extrapolation of the cross section [18].

(2) There are measurements [19] for the $d(\alpha,\gamma)^6$Li fusion at energies above 1 MeV. They allow a comparison with the results extracted from Coulomb dissociation.

(3) The first excited state of ^{6}Li [$E_x(3_1^+)=2.19$ MeV] lies 710 keV above the breakup threshold. Since the resonance strength (reduced transition probability) is experimentally well known [20] and the Coulomb excitation theory for quasibound states appears to be reliable, the observation of the sequential breakup checks the anticipated electromagnetic reaction mechanism and provides information on possible interferences from spurious nuclear contributions [21].

(4) Because of the identical charge-to-mass ratios of ^{6}Li projectiles, α particle and deuteron fragments postacceleration effects with distortions of the kinematics at the breakup point are minimized.

First of all, the present paper describes the experimental method and procedures in detail. The results demonstrate the feasibility of such experiments and give an experimental basis of refined theoretical analyses. The first analyses of the cross sections prove the dominance of the Coulomb breakup mechanism and define the conditions most favorable for extracting information on radiative capture reactions. The observed direct (nonresonant) Coulomb breakup confirms experimentally the theoretically accepted value of the astrophysical S factor [19] for the thermonuclear fusion of α particles and deuterons.

II. REACTION KINEMATICS

For measurements of Coulomb breakup reactions with small relative energies between the fragments, especially in the domain of astrophysical energies (typically some keV up to some hundred keV), but fairly large laboratory fragment energies, very specific demands are set to the detection system. As the peculiarities for this type of studies hold in general for many projectile-fragment combinations, some specific aspects of the reaction kinematics will be discussed with focus on the present experiment.

A. Trajectories

In a classical treatment the most characteristic signature for a nuclear reaction being governed by the Coulomb interaction is the pure Rutherford trajectory of the scattered particle. In the case of a binary breakup reaction, the projectile and—after breakup—the center of mass of the fragments have to follow this track. At center-of-mass energies far above the Coulomb barrier, this condition is approximately fulfilled at reaction angles between 0° and the grazing angle. This corresponds to impact parameters for which the minimum distance between projectile and target nucleus is larger than the sum of their nuclear radii. At the grazing angle the nuclei are just touching each other and the deflection due to Coulomb interaction is largest. At slightly smaller impact parameters, the attractive nuclear force partly balances the repulsive Coulomb force. Hence the asymptotic trajectories look like pure Rutherford ones with larger impact parameters, but leading to smaller scattering angles. In this angular range where both kinds of trajectories can contribute, the constructive interference leads to an enhancement of the elastic-scattering cross section σ_{el} above the Rutherford cross section σ_R. This is signaled in the angular distribution by a broad bump just below the grazing angle, where σ_{el}/σ_R reaches values above unity, sometimes called the "Coulomb rainbow."

In earlier experiments [11], the elastic scattering of 156 MeV ^{6}Li incident on ^{208}Pb was measured in the angular range of 5°–30°. Although the grazing angle is about 10° when calculated with realistic nuclear radii, the Coulomb rainbow region extends down to 7°. Hence pure Rutherford scattering can be expected only below 7°. As in the case of elastic scattering, it is reasonable to assume that also elastic breakup reactions are practically exclusively due to the Coulomb interaction if the scattering angles of the center of mass of the fragments are below the Coulomb rainbow. Here elastic breakup characterizes the projectile breakup where the target nucleus is staying in the ground state. This assumption may be understood on the basis of classical trajectory calculations [5]. They indicate that trajectories which have small impact parameters and are deflected inside the Coulomb rainbow by the nuclear potential do not contribute to *elastic* breakup due to the strong nuclear absorption. However, this remains a question to be experimentally investigated in more detail. For this purpose the resonant breakup has been measured in small angular steps between 1.5° and 6°. By a careful analysis of these data, the influence of Coulomb and nuclear interaction was studied for scattering angles below the Coulomb rainbow (see Ref. [21]).

B. Projectile breakup kinematics

The restriction to small scattering angles and the large difference in mass number of target and projectile leads to negligible target recoil energies for the studied reaction. This means that the reaction Q value is determined only by the breakup threshold of the projectile Q_{th} and by the excitation energy E_x of the target nucleus. With E_{sum} being the sum of the kinetic energies of the fragments, one gets

$$E_{sum}=E_{proj}-Q_{th}-E_x \ . \tag{2.1}$$

By measuring the energies of both fragments in a detection system with good energy resolution, elastic breakup events can easily be identified and separated from other reaction paths. This is considerably facilitated by the relatively high excitation energy of the first excited state in ^{208}Pb (2.6 MeV). The kinetic energy in the exit channel, which is shared by the two fragments, has a constant value independent of detection angles and relative energies between the fragments. As shown in Fig. 1 for a typical detection angle setting, the kinematical loci of deuteron and α particle energy for elastic breakup form a straight line. Indicated on this curve are the two kinematical loci for the resonant breakup via the first excited state in ^{6}Li at 2.19 MeV, located at 0.71 MeV above the α-d breakup threshold. The two different combina-

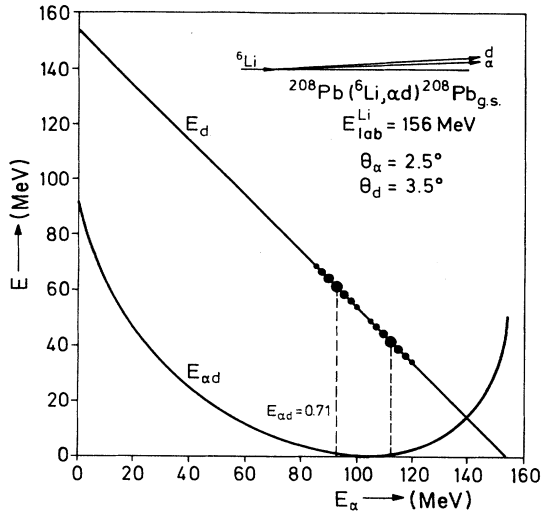

FIG. 1. Laboratory energy of the deuteron and relative energy between the fragments as a function of the α particle laboratory energy for the elastic breakup of ^{6}Li. The α particle energies for the two loci of resonant breakup of ^{6}Li via the 2.19-MeV state with the relative energy $E_{\alpha d}=0.71$ MeV are indicated.

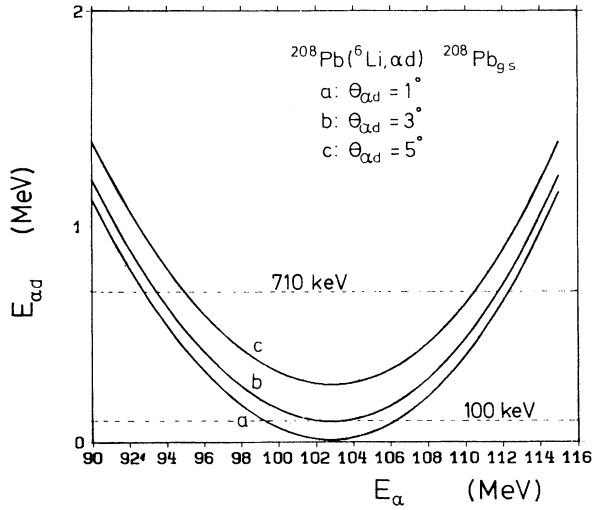

FIG. 2. Relative energy as a function of the α particle laboratory energy for the elastic breakup of 156 MeV ^{6}Li projectiles at three different relative angles between the fragments.

tions of α particle and deuteron energy correspond to breakup events, where the α particle is emitted with a velocity component in direction of the momentum vector of the excited ^{6}Li and the deuteron with a component backward and vice versa, respectively. The relative energy curve, which is also given in this figure, shows that two combinations are possible for a wide range of relative energies.

An interesting feature is the remarkably slow variation of the relative energy $E_{\alpha d}$ around its minimum as compared to the laboratory energies of the fragments. This so-called "magnifying glass effect" leads to a very good energy resolution of the relative energy, even with moderate laboratory energy resolution. The effect is due to various cancellations of different terms in the expression of the relative energy or the relative velocity $v_{\alpha d}$, respectively. With

$$v_{\alpha d}^2=v_\alpha^2+v_d^2-2v_\alpha v_d\cos\Theta_{\alpha d}\ , \tag{2.2}$$

one derives

$$v_{\alpha d}dv_{\alpha d}=(v_\alpha-v_d\cos\Theta_{\alpha d})dv_\alpha+(v_d-v_\alpha\cos\Theta_{\alpha d})dv_d\ .$$

Therefore, for beam velocity particles ($v_\alpha\approx v_d$) emitted in a narrow angle cone ($\cos\Theta_{\alpha d}\approx 1$), the relationship

$$dE_{\alpha d}\ll dE_\alpha, dE_d \tag{2.3}$$

holds.

At $E_{\alpha d}=100$ keV, for example, a change of 10 keV in the relative energy corresponds to a change of 200 keV for the laboratory fragment energies. On the other hand, however, a good knowledge of the relative angle between the fragments is required to maintain a good relative energy resolution:

$$dE_{\alpha d}=\frac{2\sqrt{m_\alpha m_d E_\alpha E_d}}{m_\alpha+m_d}\sin\Theta_{\alpha d}\,d\Theta_{\alpha d}\ . \tag{2.4}$$

This situation is illustrated in Fig. 2, which shows the relative energy as a function of the α particle energy for different relative angles. First of all, Fig. 2 verifies that relative angles of less than 3° are necessary to approach relative energies below 100 keV. Concerning the required angular resolution, one deduces that at $E_{\alpha d}=100$ keV an uncertainty of 2° leads to an uncertainty of 50 keV in the relative energy.

In summary, out of the variety of possible detector settings, the best configuration should be carefully chosen, according to the relative energy range and resolution of the planned experiment.

III. EXPERIMENTAL SETUP AND PROCEDURES

A. Principle of measurements

For the coincident detection of the two breakup fragments, a single-arm magnetic spectrograph was used. This is the only instrument to achieve a sufficiently small scattering angle and sufficiently small relative angles between the fragments. As indicated in Fig. 3, both fragments enter the same angular acceptance space of the spectrograph defined by adjustable crossed slits. Breakup particles with slightly different momenta (i.e., with nonzero relative energy) are separated in the dispersive magnet system independent of their relative emission angles. As a result of this "automatic" separation of the fragments, they can be detected in coincidence using a two-part detection system in the focal plane of the spectrograph. The example in Fig. 3 shows only the case where the deuteron has a lower momentum than the α particle. Of course, also the reversed case can simultane-

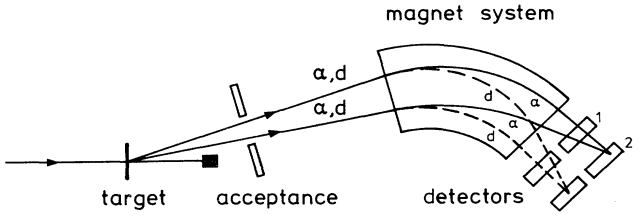

FIG. 3. Experimental arrangement for coincident detection of binary breakup fragments using a magnetic spectrograph.

ously be detected with such a setup.

The more difficult task in this experimental arrangement is the measurement of the relative emission angles between the particles which also enter the determination of the relative energy as discussed above. Two methods to deal with this problem have been applied in different phases of the experimental efforts.

The simple method is to reduce the angular acceptance of the spectrograph considerably and use a fixed value for the relative emission angle deduced from Monte Carlo simulations of the corresponding geometry [22]. In this procedure the uncertainty of the deduced relative energy of the fragments depends only on the chosen limited acceptance angle and can be calculated from it (see below). The obvious disadvantage of the method is the reduced detection efficiency which scales with the square of the acceptance solid angle. Therefore, a direct measurement of the relative emission angles was pushed forward.

Several methods do, in principle, exist to detect the emission angle of each particle. One of these is to place a two-dimensional position-sensitive detector in front of the magnet system, e.g., close to the position of the acceptance slit. Two different prototypes of such detectors, a parallel-plate avalanche detector and a multiwire proportional chamber, have been used for test purposes [16,23]. Angular resolutions better than 5 mrad have been achieved with these detectors. However, it turned out that they could hardly be used for the coincidence measurements due to count-rate problems. In order to achieve a sufficiently high coincidence count rate, the beam intensity had to be chosen as high as possible. Hence the count rate of elastically scattered ^{6}Li particles was increased so much that these acceptance detectors were overloaded. The separation of the small signals from penetrating deuterons in the presence of a high count rate from large Li pulses aggravated these problems also at lower beam intensities. Moreover, the detector material caused a considerable energy and angular straggling, which deteriorated the momentum resolution of the spectrograph.

In the focal plane the high background of elastically scattered ^{6}Li particles could be suppressed by a simple method. Since these particles have nearly the same magnetic rigidity as a pair of breakup particles with zero relative energy, they pass the focal plane of the spectrograph just at that position where the two independent focal-plane detector systems touch. Hence the ^{6}Li particles were stopped by a graphite block at this position. Since only downstream of this graphite absorber active detectors could be placed, the remaining method for detecting the relative emission angles was to measure the particle tracks in this region of the setup using two planes of position-sensitive detectors (Fig. 3) and to calculate the full trajectory from the target by ion optical methods as described below. This method of particle-particle correlation measurements has been proposed [24] in detail in 1986 in context with the application of the spectrograph "Little John" and its feasibility was demonstrated in Ref. [25]. Recently, Utsunomiya, Lui, and Schmitt [26] discussed the applicability of a two-part focal-plane detector for various studies.

B. Magnetic spectrograph and experimental environment

The measurements were performed at the Karlsruhe Isochronous Cyclotron using the magnetic spectrograph "Little John" [16] for detection of the breakup fragments. The external ECR ion source LISKA [27] specially designed for Li ions provided an intense beam of $^6Li^{3+}$ particles, which were axially injected into the cyclotron and accelerated to a beam energy of 156 MeV. After analysis in a conventional monochromator magnet, a beam intensity up to 0.1 μA was available at the target with an energy spread of less than 100 keV. Very stable beam intensities were of great advantage for the coincidence measurements. With a bunching system used in the injection line to the cyclotron, a 11-MHz time structure synchronized with the 33-MHz operating frequency of the cyclotron was prepared. This was leading to a suppression of accidental coincidences between particles from different bunches due to flight-time differences.

The beam was focused in the target plane to a spot of about 1 mm in size and with an angular divergence of about 2 mrad. Position control of the target spot on the optical axis of the spectrograph was provided by a laser system.

The magnetic spectrograph has a QQDS (quadrupole-quadrupole-dipole-sextupole) magnet configuration with a 60° deflecting dipole magnet of 1.5 m curvature radius. With a maximum field strength of more than 1.7 T, the bending power exceeds 2.5 T m, being sufficient to deflect deuterons of 150 MeV energy. The field strength of the dipole is controlled with an accuracy of some 10^{-4} by a temperature-stabilized Hall probe. The two quadrupole magnets provide flexible focusing conditions, leading to a variable momentum acceptance and resolution, respectively [16]. With the sextupole magnet the focal plane is turned to the correct inclination for each operation mode. The mode with largest momentum acceptance and lowest resolution was chosen in the present experiments. In this mode the focal plane is congruent with proportional counter 1 closest to the sextupole magnet, as shown in Fig. 4. Proportional counter 1, which is necessary for particle tracking as discussed above, was used only in the later phase of experiments. In the former phase the detector part far downstream consisting of one proportional counter (counter 2 in Fig. 4), ionization chamber, and scintillator was completely shifted to a position such that the proportional counter was approximately at the position of counter 1 in Fig. 4.

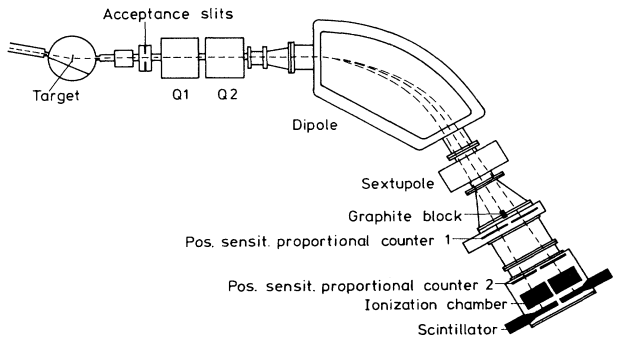

FIG. 4. Karlsruhe magnetic spectrograph "Little John" with two-part detector system for coincident detection of breakup fragments.

The two identical proportional counterparts of counter 1 provided the momentum information by measuring the particle position via charge division at a thin resistive wire. In the vertical direction the position was determined by a drift-time measurement of the electron signal from the wire with respect to a fast start signal from the scintillator. The ionization chambers measured the energy loss of the penetrating particles and the scintillators the remaining energy. Hence particle identification was provided by the usual ΔE-E technique. The design and operation conditions of each detector stack were as previously described [16] for the singlefold types covering the full focal plane.

At reaction angles $\geq 3°$, the primary ^{6}Li beam was stopped in a slightly shielded Faraday cup with a δ-electron repeller inside the target chamber (inner diameter of 50 cm). For monitoring purposes the accumulated charge could be measured quite reliably with this device. At smaller reaction angles a specially prepared wedge of the acceptance slit served as beam stop. However, a reproducible beam monitoring over many long-lasting beam times was not possible with it. Therefore, an additional monitor detector was mounted at a fixed scattering angle inside the target chamber. It consisted of a CsI scintillation crystal with photodiode readout. The peak of elastically scattered ^{6}Li particles was differentially discriminated and its counts were scaled.

The detector electronics consisted of standard NIM modules and the data readout was done with a CAMAC system connected to an LSI 11/73 minicomputer operated under RT11. Before the main particle-particle correlation coincidence circuit, two independent coincidences, including each detector of both stacks, were connected to reduce neutron- and gamma-induced background.

C. Procedures

The data presented in this work have been collected in seven beam periods of 1 week each distributed over 24 months. The ^{208}Pb targets used were self-supporting metallic foils of 4.0 and 6.7 mg/cm^2 thickness, respectively, and an isotope enrichment $>99\%$. At the beginning of each beam period, the direction of the beam with respect to the angular scale of the spectrograph was determined by a method previously described [11]. Therefore, the absolute scattering angle scale was known with an accuracy better than $\pm 0.05°$.

This was followed by the usual calibration measurements for the slightly nonlinear relation between position signal and particle momentum. This calibration is very important for the present experiment, since the shape of a continuous spectrum is to be measured. Because of different signal response of the position-sensitive detectors to different particle types, the calibration had to be done in two steps. First, for the fixed and well-known momentum of elastically scattered ^{6}Li particles, the relation position versus magnetic-field strength was measured for 15–20 different field-strength settings equally distributed over the full momentum acceptance. The magnetic-field strength was then for all particle types related to the true position in the focal plane by putting a diaphragm with a row of slits in front of the position detectors and sweeping the reaction products from a ^{12}C target across it [22].

Also of great importance were careful total transmission measurements since the spectrograph was operated slightly outside its design specifications [16] concerning momentum and angular acceptance range. Therefore, the transmission was lower than 100% for particles with momenta close to the acceptance limit and with large emission angles [22,28]. The transmission measurements were done in parallel with the first step of the momentum calibration using the CsI monitor detector as a reference. The angular acceptance was derived from comparison of corresponding measurements with small and large acceptance slit widths [22]. The detection efficiency for different particles was corrected off-line after the experiment runs by renormalization as described below.

In case of measurements with the additional position-sensitive detector for particle tracking and determination of the relative emission angles, an additional angular calibration was necessary. This was performed by setting a small horizontal/vertical slit at different vertical/horizontal positions covering the full acceptance range and measuring the corresponding angle of the track of elastically scattered ^{6}Li particles in the focal plane. This calibration had to be done for a set of particle momenta covering the momentum acceptance since the ion optical angular imaging coefficients depend on the particle's momentum [29]. As in the case of the momentum calibration, elastically scattered ^{6}Li particles were used for this purpose and the magnetic field was set to different values to cover the focal plane. These calibration procedures had been repeated during some of the runs. However, it turned out that it was only necessary to control the magnetic-field strength and correct for its drifts.

At the beginning and end of a measuring run, all important parameters such as spectrometer angular setting, target number, acceptance slit position, and width were recorded on tape. During the runs, in addition to the detector signals, the magnetic-field strength and accumulated beam charge, the monitor detector scaler, and vari-

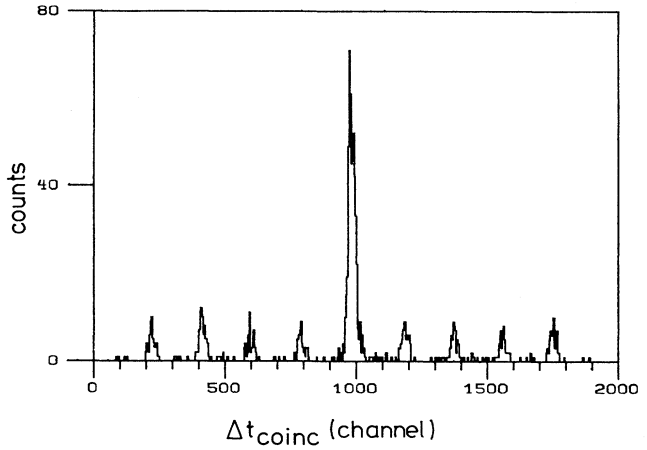

FIG. 5. Time-difference spectrum for coincidences between the left and the right part of the focal plane detector. The pulsed structure of the Li beam is clearly revealed. True coincidences are contained in the large peak, considerably dominating over the small peaks from accidental coincidences.

ous scalers of the single detector rates were recorded in each data block for control of a proper function of the system. For normalization purposes the single-event spectra from each of the two-part detector systems were recorded after being down scaled at a rate of $\frac{1}{256}$. Control of the beam position and direction was given by various passive and active slit systems in the beam line, which were carefully adjusted after beam focusing. Further details about the experimental setup and procedures are given in Ref. [22].

IV. DATA EVALUATION AND RESULTS

A. Data processing

The α-d breakup reactions of interest were selected by setting the appropriate windows in the $\Delta E/E_{\text{rest}}$ spectra and in the time-difference spectrum (Fig. 5) for coincidence events between the left and right part of the focal-plane detector. A kinematical plot for such events is shown in Fig. 6. Most events were accumulated along

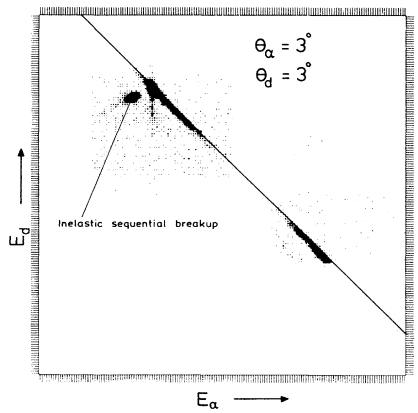

FIG. 6. Two-dimensional plot of α-particle–deuteron coincidences in the focal-plane detector. The line for constant sum energy $E_{\text{sum}}=154.5$ MeV is indicated.

TABLE I. Resolution on the scale of the relative energy with realistic experimental conditions (acceptance 20×30 mrad^2, target thickness 4 mg/cm^2) from Monte Carlo simulations.

Relative energy (keV)	Resolution (FWHM) (keV)
100	19
300	27
500	40

the line of constant sum energy $E_{\text{sum}}=154.5$ MeV, which is attributed to elastic breakup. The upper left part of the line corresponds to α particles in the left part of the detector and deuterons in the right part, which are breakup events with emission of the deuteron in the direction of the center-of-mass motion. The inverse combination, backward emission of the deuteron, holds for the lower right part of the line. The gap in between, which is the region of very small relative energies, was due to the extremely low breakup cross section for relative energies around 0 and the dead zone between the detectors, which covered this region of relative energies, as already described above (Sec. III). An additional accumulation of events in the upper left part below the line for elastic breakup originated from resonant breakup of ^{6}Li with additional excitation of ^{208}Pb target nuclei ($E_x=2.6$ MeV). Observation of this inelastic resonant breakup has been reported elsewhere [30] and will not be considered in the present analysis. The experimental cross sections are added in the compilation of Table II.

For the further analysis, elastic breakup is selected by setting a sum energy window $E_{\text{sum}}=154.3\pm1.1$ MeV, which is 200 keV less than the kinematical value due to energy loss in the target. The relative energy spectra were generated by a relativistic event-by-event transformation of the laboratory energies and relative angle to the energy in the center of mass of the fragments. For

TABLE II. Double-differential $d^2\sigma/d\Omega_{\text{Li}^*}d\Omega_{ad}$ ($=\sigma_2$) and single-differential $d\sigma/d\Omega_{\text{Li}^*}$($=\sigma_1$) cross sections of the elastic and inelastic resonant breakup reaction ^{208}Pb (^{6}Li, ^{6}Li$^*_{2.19\text{ MeV}}\rightarrow\alpha d$)^{208}Pb$_{\text{g.s.}}$(^{208}Pb$^*_{2.61\text{ MeV}}$). The experimental uncertainties are given in parentheses.

$\Theta_{\text{c.m.}}$ (deg)	σ_2 (elastic) (mb/sr^2)		σ_1 (elastic) (mb/sr)		σ_1 (inelastic) (mb/sr)	
1.5	7.2	(2.8)	61	(24)		
2.1	5.02	(0.71)	45.3	(6.4)	8.3	(2.0)
2.6	9.32	(0.61)	96.4	(6.3)	12.6	(2.1)
3.1	13.80	(0.55)	159.7	(6.4)	11.9	(1.7)
3.6	7.90	(0.65)	101.6	(8.4)	10.5	(2.5)
3.7	7.63	(0.97)[a]	100.7	(12.8)		
4.1	12.46	(0.40)	177.4	(5.7)	3.7	(0.8)
	12.3	(1.0)[a]	175.6	(14.2)		
4.5	13.38	(0.99)[a]	206.1	(15.3)		
5.2	14.60	(0.59)	254.7	(10.3)	3.6	(1.0)
6.2	10.08	(0.40)	215.3	(5.0)	1.5	(0.6)

[a]Measured with different setup (see Ref. [28]).

cases where information on the relative angle was missing, a fixed relative angle was used, as it results as the mean relative angle from a Monte Carlo simulation of the experiment [22].

B. Results

An example of a relative energy spectrum taken at a mean reaction angle of 3° is shown in Fig. 7(a), where the negative-energy axis denotes breakup with backward emission of the α particles. For these reactions the peak due to resonant breakup at $E_{\alpha d}=710$ keV can clearly be identified as well as direct breakup to energies below 100 keV. It should be noted that the detection limit for relative energies of about 50 keV is not due to detector limitations, but due to statistics, as the spectrum may indicate. For the positive-energy branch corresponding to forward emission of the α particle, direct breakup particles were observed only up to a relative energy of 600 keV. This resulted from the slightly asymmetrical momentum acceptance of the spectrograph with respect to the central trajectory. Therefore, backward-emitted resonant breakup deuterons, which have a momentum deviation from the central trajectory that is twice as large as backward-emitted α particles, were not accepted by the spectrograph.

All spectra are corrected for the background of random coincidences. This background was inferred from the random peaks in the time-difference spectrum (Fig. 5) in exactly the same way as the true coincidences. It was less than 0.1% for the resonance peak and became only important (> 10%) below 100 keV.

The resolution on the relative energy scale was determined with the above-mentioned Monte Carlo simulation program. Table I gives the results of the simulation for several relative energies. A check of this procedure was provided by the very good reproduction of the resonance peak, using the experimental conditions and the well-known natural width of this resonance state.

For comparison with theory the triple-differential laboratory cross sections $d^3\sigma/d\Omega_\alpha d\Omega_d dE_{\alpha d}$ are converted to the c.m. cross sections $d^3\sigma/d\Omega_{\mathrm{Li}^*}d\Omega_{\alpha d}dE_{\alpha d}$ by kinematical transformation described in Ref. [31]. Figure 7(b) shows the transformed spectrum of Fig. 7(a). The much steeper slope of the cross section toward small energies is due to the rapid decrease of the transformation factor for very small energies. This enabled us to obtain a relative energy spectrum where the values of the triple-differential cross section extend over more than three orders of magnitude with reasonable statistics (Tables III–VI). The spectra shown in Fig. 7 result from a full-week measuring period, using an angular acceptance of the spectrograph $\Omega_\alpha=\Omega_d=20$ mrad (horizontal)×30 mrad (vertical). It has been reproduced by a further run at the same scattering angle with a different target and an angular acceptance of 7×34 mrad^2. Both data sets agree over the whole range of relative energies within the statistical uncertainty.

Besides the spectra taken at $\Theta_\alpha=\Theta_d=3°$, the angular range from 1.5° to 6° has been investigated in steps of 0.5°–1°. Because of the lower statistics of these data, only the sequential breakup is used for the analysis. It has been extracted by an integration from 600 to 800 keV over the resonant peak at 710 keV, subtracting the direct breakup contribution, which was linearly interpolated between 600 and 800 keV. The resulting double-differential cross sections $d^2\sigma/d\Omega_{\mathrm{Li}^*}d\Omega_{\alpha d}$ are listed in Table II together with the differential cross sections $d\sigma/d\Omega_{\mathrm{Li}^*}$. They have been obtained by integrating over $\Omega_{\alpha d}$ assuming an angular distribution of the fragment emission in the ^{6}Li* system for a pure $E2$ Coulomb excitation mechanism [32].

TABLE III. Triple-differential cross section $d^3\sigma/d\Omega_\alpha d\Omega_d dE_{\alpha d}$ $(=\sigma_3)$ of the elastic breakup reaction ^{208}Pb(^{6}Li,αd)^{208}Pb$_{\mathrm{g.s.}}$: $\Theta_{\mathrm{lab}}=2°$. Negative signs of $E_{\alpha d}$ denote the branch with $v_\alpha < v_d$.

$E_{\alpha d}$ (MeV)	σ_3 (mb/sr^2 MeV)	$(\Delta\sigma_3)$
−0.85	462	(267)
−0.83	153	(153)
−0.81	153	(153)
−0.79	304	(215)
−0.77	604	(302)
−0.75	1655	(499)
−0.73	3747	(749)
−0.71	4180	(790)
−0.69	1339	(446)
−0.67	2668	(629)
−0.65	886	(362)
−0.63	884	(361)
−0.61	587	(294)
−0.59	586	(293)
−0.57	730	(327)
−0.55	146	(146)
−0.53	145	(145)
−0.51	145	(145)
−0.49	242	(210)
−0.43	288	(203)
−0.41	144	(144)
−0.39	287	(203)
−0.37	429	(248)
−0.33	143	(143)
−0.31	285	(201)
−0.29	142	(142)
−0.27	142	(142)
−0.25	284	(201)
0.25	135	(135)
0.33	135	(135)
0.35	540	(270)

The angular distribution of the differential cross section for this elastic sequential breakup is presented in Fig. 8. Data from 1.5° to 6° represented by crosses are all measured during one experimental period with the same beam conditions, target, and detector setup, thus minimizing the errors in the relative normalization of the cross sections. For the data from 3° to 6°, the integrated beam current collected in a shielded Faraday cup inside the target chamber served for the normalization. The stability of this measurement was checked by the CsI scintillator monitor detector mounted at ≈20° scattering angle. The

TABLE IV. Triple-differential cross section $d^3\sigma/d\Omega_\alpha d\Omega_d dE_{\alpha d}$ $(=\sigma_3)$ of the elastic breakup reaction ^{208}Pb(^{6}Li,αd)^{208}Pb$_{g.s.}$: $\Theta_{lab}=3°$. Negative signs of $E_{\alpha d}$ denote the branch with $v_\alpha < v_d$.

$E_{\alpha d}$ (MeV)	σ_3 (mb/sr^2 MeV)	$(\Delta\sigma_3)$	$E_{\alpha d}$ (MeV)	σ_3 (mb/sr^2 MeV)	$(\Delta\sigma_3)$
−1.01	23	(17)	−0.23	225	(45)
−0.99	23	(16)	−0.21	144	(37)
−0.97	80	(30)	−0.19	250	(48)
−0.95	22	(16)	−0.17	119	(35)
−0.93	44	(22)	−0.15	129	(35)
−0.91	52	(25)	−0.13	126	(35)
−0.89	75	(28)	−0.11	140	(38)
−0.87	72	(28)	−0.09	62	(30)
−0.85	39	(21)	−0.07	14	(22)
−0.83	215	(48)	−0.05	27	(26)
−0.81	269	(53)	0.07	37	(22)
−0.79	464	(69)	0.09	79	(27)
−0.77	1484	(122)	0.11	61	(25)
−0.75	4530	(212)	0.13	92	(30)
−0.73	8121	(283)	0.15	210	(42)
−0.71	6921	(260)	0.17	130	(34)
−0.69	4064	(198)	0.19	247	(46)
−0.67	2186	(145)	0.21	275	(48)
−0.65	1570	(123)	0.23	265	(47)
−0.63	1027	(99)	0.25	345	(54)
−0.61	760	(84)	0.27	239	(45)
−0.59	865	(90)	0.29	323	(52)
−0.57	657	(79)	0.31	280	(48)
−0.55	761	(84)	0.33	319	(52)
−0.53	625	(76)	0.35	362	(55)
−0.51	709	(80)	0.37	309	(51)
−0.49	456	(65)	0.39	272	(49)
−0.47	589	(73)	0.41	406	(58)
−0.45	444	(63)	0.43	365	(55)
−0.43	453	(63)	0.45	419	(59)
−0.41	341	(55)	0.47	452	(61)
−0.39	376	(59)	0.49	454	(62)
−0.37	253	(49)	0.51	383	(56)
−0.35	284	(50)	0.53	440	(61)
−0.33	221	(47)	0.55	418	(59)
−0.31	303	(51)	0.57	445	(61)
−0.29	289	(51)	0.59	149	(35)
−0.27	292	(51)	0.61	81	(26)
−0.25	226	(46)			

relation between the rate of elastically scattered projectiles and the accumulated charge was constant within 4.5% for the data set from 3° to 6°.

A different normalization procedure had to be applied for the reaction angles 1.5°, 2°, and 2.5°, where the beam was stopped on the acceptance slits (see Sec. III). A normalization relative to the data at larger angles with the help of the monitor detector was not possible because of different background conditions. For these data simultaneously registered inclusive particle spectra were used for the normalization. In previous experiments [11] with the spectrometer, these inclusive spectra had already been measured in the same angular region. The comparison of these reference data with the actual inclusive data at 3°–6° showed an agreement better than 10%. For the overall absolute cross-section normalization, an uncertainty of 15% is estimated, taking into account the uncertainty in the target thickness and detection efficiency.

The sharp dip in the angular distribution at 3.5° has been fully confirmed in another experimental run, where the data at 3°, 3.5°, and 4° were remeasured. All of the above-described data for sequential breakup have been taken with the detector setup without relative angle information, thus using a small aperture of the spectrograph $\Omega_\alpha=\Omega_d=9\times40$ mrad^2, except at 1.5°, where 9×10 mrad^2 was used. Additional data between 3.6° and 4.4°—indicated as squares in Fig. 8—have been obtained with the extended detector setup, which provided a determination of the emission angles of the fragments. Here the acceptance of 20×30 mrad^2 of the spectrometer was subdivided off-line [28] into three bins, providing the data points at 3.6°, 4°, and 4.4°. Again, the excellent agree-

TABLE V. Triple-differential cross section $d^3\sigma/d\Omega_\alpha d\Omega_d dE_{\alpha d}$ $(=\sigma_3)$ of the elastic breakup reaction ^{208}Pb(^{6}Li,αd)^{208}Pb$_{g.s.}$: $\Theta_{lab}=4°$. Negative signs of $E_{\alpha d}$ denote the branch with $v_\alpha < v_d$.

$E_{\alpha d}$ (MeV)	σ_3 (mb/sr^2 MeV)	$(\Delta\sigma_3)$	$E_{\alpha d}$ (MeV)	σ_3 (mb/sr^2 MeV)	$(\Delta\sigma_3)$
−1.09	69	(49)	−0.47	268	(89)
−1.07	69	(48)	−0.45	237	(84)
−1.05	68	(48)	−0.43	247	(90)
−1.03	135	(67)	−0.41	256	(89)
−1.01	123	(68)	−0.39	256	(89)
−0.99	299	(100)	−0.37	246	(90)
−0.97	66	(47)	−0.35	196	(78)
−0.95	164	(73)	−0.31	108	(60)
−0.93	162	(73)	−0.29	235	(83)
−0.91	194	(79)	−0.27	107	(59)
−0.89	278	(97)	−0.25	68	(52)
−0.87	223	(84)	−0.23	97	(60)
−0.85	317	(100)	−0.21	175	(71)
−0.83	274	(95)	−0.19	58	(53)
−0.81	346	(104)	−0.17	68	(52)
−0.79	845	(163)	−0.15	48	(42)
−0.77	1983	(249)	−0.13	39	(43)
−0.75	6109	(435)	−0.11	58	(53)
−0.73	9162	(532)	−0.09	97	(60)
−0.71	8214	(503)	−0.07	19	(45)
−0.69	6345	(441)	−0.03	29	(44)
−0.67	2444	(273)	0.21	28	(28)
−0.65	1431	(209)	0.23	74	(49)
−0.63	840	(161)	0.25	213	(79)
−0.61	605	(135)	0.27	167	(68)
−0.59	634	(138)	0.29	93	(57)
−0.57	572	(131)	0.31	185	(74)
−0.55	470	(120)	0.33	250	(83)
−0.53	619	(138)	0.35	130	(63)
−0.51	388	(108)	0.37	158	(69)
−0.49	229	(85)			

TABLE VI. Triple-differential cross section $d^3\sigma/d\Omega_\alpha d\Omega_d dE_{\alpha d}$ $(=\sigma_3)$ of the elastic breakup reaction ^{208}Pb(^{6}Li,αd)^{208}Pb$_{g.s.}$: $\Theta_{lab}=6°$. Negative signs of $E_{\alpha d}$ denote the branch with $v_\alpha < v_d$.

$E_{\alpha d}$ (MeV)	σ_3 (mb/sr^2 MeV)	$(\Delta\sigma_3)$	$E_{\alpha d}$ (MeV)	σ_3 (mb/sr^2 MeV)	$(\Delta\sigma_3)$
−1.09	71	(50)	−0.73	8820	(529)
−1.07	141	(70)	−0.71	6606	(457)
−1.05	175	(78)	−0.69	4062	(358)
−1.03	173	(77)	−0.67	2259	(266)
−1.01	103	(59)	−0.65	938	(171)
−0.99	239	(90)	−0.63	530	(129)
−0.97	271	(96)	−0.61	466	(120)
−0.95	157	(76)	−0.59	527	(128)
−0.93	134	(67)	−0.57	340	(103)
−0.91	332	(105)	−0.55	339	(102)
−0.89	396	(114)	−0.53	62	(44)
−0.87	164	(73)	−0.51	215	(81)
−0.85	457	(122)	−0.49	20	(32)
−0.83	584	(138)	−0.47	92	(53)
−0.81	517	(129)	−0.45	183	(75)
−0.79	1285	(203)	−0.43	61	(43)
−0.77	1941	(250)	−0.41	142	(69)
−0.75	5012	(401)	−0.39	152	(68)

TABLE VI. (*Continued*).

$E_{\alpha d}$ (MeV)	σ_3 (mb/sr^2 MeV)	$(\Delta\sigma_3)$	$E_{\alpha d}$ (MeV)	σ_3 (mb/sr^2 MeV)	$(\Delta\sigma_3)$
−0.37	121	(61)	−0.15	10	(33)
−0.35	81	(53)	−0.13	20	(31)
−0.33	91	(52)	−0.09	20	(31)
−0.31	30	(30)	0.23	67	(51)
−0.29	110	(61)	0.25	162	(71)
−0.27	50	(44)	0.27	95	(59)
−0.25	60	(42)	0.29	124	(65)
−0.23	30	(30)	0.31	67	(51)
−0.21	120	(60)	0.33	124	(65)
−0.19	30	(46)	0.35	133	(65)
−0.17	40	(45)	0.37	57	(40)

ment with the other data confirms the reproducibility of the breakup measurements with different detection systems and methods.

V. ANALYSIS

The sequential breakup mode and measured differential cross section for the excitation of the 3_1^+ state of the ^{6}Li projectile have been recently [21] analyzed on equal footing with Coulomb and nuclear excitation in the framework of a full coupled-channel approach. Adopting the value of the electromagnetic transition probability $B(E2;1^+\rightarrow 3^+)=21.8\ e^2\text{fm}^4$ experimentally known from (e,e') scattering [33], the analysis has been performed with the view of possible effects arising from the nuclear interaction. The results demonstrated convincingly the dominance of the Coulomb interaction for the *elastic* breakup of the projectile scattered into the very forward region. The angular region of the differential cross section below half the grazing angle proved to be practically unaffected by nuclear contributions. In principle, such contributions could be present even at the most forward angles. Their disappearance for *elastic* breakup is a consequence of the strong absorption of trajectories with small impact parameters associated with small deflection angles [5,21].

The case of nonresonant Coulomb dissociation is theoretically more complicated as—unlike the sequential breakup—the regions of excitation and disintegration are not well separated [2]. Thus "post acceleration" or final-state interactions in the Coulomb field of the target (see Fig. 9) may distort a simple relationship between the cross section and electromagnetic matrix elements of the projectile structure and astrophysical S factor, respectively.

Concerning the kinematical effects of post acceleration, the necessary corrections mapping the asymptotic kinematics to that of the breakup locus appear similar to procedures used in nuclear interferometry in heavy-ion reactions [34]. In the present case of ^{6}Li breakup with frag-

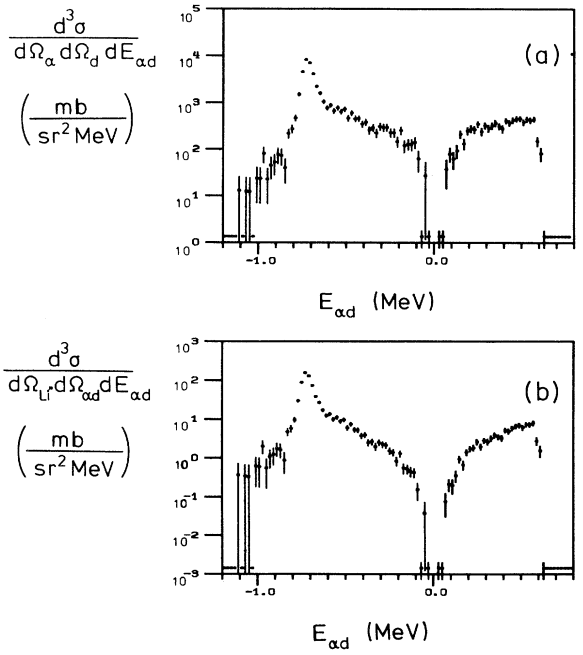

FIG. 7. Triple-differential cross section for elastic breakup of ^{6}Li in the (a) laboratory system and (b) center-of-mass system of the fragments as a function of relative energy. Negative and positive relative energies denote backward and forward emission, respectively, of the α particle in the ^{6}Li c.m. system.

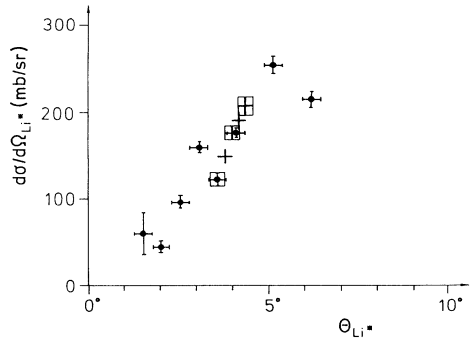

FIG. 8. Measured angular distribution of the reaction ^{208}Pb(^{6}Li,^{6}Li$^*_{2.19\ \text{MeV}}\rightarrow\alpha+d$)^{208}Pb$_{\text{g.s.}}$. The horizontal error bars correspond to the angular acceptance $\Delta\Theta_{\text{Li}^*}$ of the spectrograph. The vertical error bars comprise the statistical uncertainty and an estimated error due to the integration over the peak of sequential breakup.

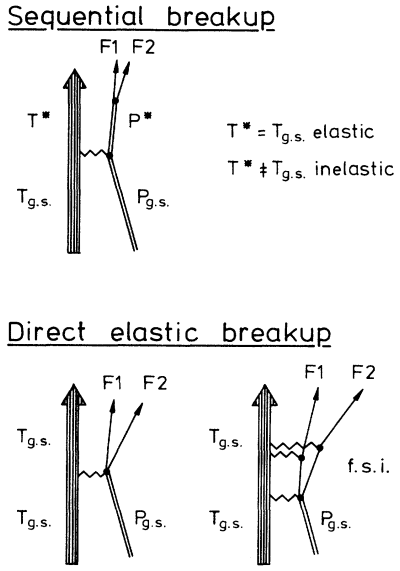

FIG. 9. Various breakup modes under consideration.

ments of equal charge-to-mass ratio, the corrections are expected to be rather small. Results of semiclassical trajectory calculations [35] (assuming the breakup locus at the top of the Coulomb barrier) support this conjecture. High projectile energies and small relative energies alleviate the problem considerably. Nevertheless, in general, a consistent analysis of the nonresonant breakup requires at least an approximate treatment of the multistep excitation of the Coulomb continuum. This is certainly a future task of the theoretical development.

Our analysis follows the theoretical formulation given in Refs. [3,4]. There is a factorization of the coincidence cross section into a kinematical part which describes the equivalent photon spectrum (including its polarization) and into a part which absorbs the nuclear structure dependence, i.e., the radiative capture matrix elements. In general, complications may arise from the competition of different multipoles ($E1$ and $E2$, e.g., as in the case $^{16}O \rightarrow \alpha + ^{12}C$; see, e.g., Ref. [36]) or from nonzero spin values of the particle (as in our case). However, it is important to stress that the analysis of the triple-differential cross section can be done in a completely model-independent way with the electromagnetic structure matrix elements entering as free parameters.

For a first inspection of the present case, we follow the argument [37] that a d-state component of the ground state of ^{6}Li is practically negligible. Thus the angular momentum of the $\alpha+d$ motion in the continuum is $l=2$ only, which couples with the deuteron spin to $I=1$, 2, and 3. Langanke has shown [38] that the wave function can be generated by a potential independent of I. (This would not be valid in the region of the 3^+ resonant state.) With these simplifications the coincidence cross section of the nonresonant Coulomb breakup is directly proportional to the astrophysical S factor:

$$S = E\sigma_{\text{capt}}(E)\exp[2\pi\eta(E)] , \tag{5.1}$$

usually introduced in order to facilitate the extrapolation of the capture cross section σ_{capt} to low energies ($\eta = Z_1 Z_2 e^2/\hbar v$ is the Coulomb parameter). It has been already shown [4] that our data are roughly reproduced with an energy-independent value of $S = 1.7 \times 10^{-5}$ MeV mb in the range of the relative energy $E_{\alpha d}$ ($=E$) ≤ 400 keV, which is considered to be unaffected by interferences from sequential breakup. This value is in fair agreement with the extrapolation of the data of Robertson *et al.* [19] by a capture model calculation.

In addition, the astrophysical S factor has been parametrized by means of a McLaurin series:

$$S(E) = S_0 + S_1 E + 0.5 S_2 E^2 . \tag{5.2}$$

The coefficients are determined by fitting the theoretical cross section to the data, whereby the quadratic term proves to be insignificant. The result

$$S(E) = [(0.91 \pm 0.18) + (2.92 \pm 0.66)E] \times 10^{-5} \text{ MeV mb} \tag{5.3}$$

is displayed in Fig. 10.

An explicit calculation of the astrophysical S factor on the basis of a microscopic model is given in Ref. [37]. Because of the d-wave penetration, a considerable energy dependence of the S factor is found which is not reproduced by our data.

Recently [39], the role of a possible $E1$ component of the $d(\alpha,\gamma)^6$Li capture cross section has been theoretically scrutinized. An admixture comparable to the $E2$ component is estimated for astrophysical energies. The $E1$ component of the Coulomb dissociation cross section is suppressed relatively to $E2$ by a factor $k_\gamma^2 b^2 \ll 1$ with k_γ the wave number of the (equivalent) photon and b the impact parameter. Hence a dominant $E1$ component may induce considerable interference effects visible in the observed differential cross section, especially through asymmetries of the two different branches on the relative ener-

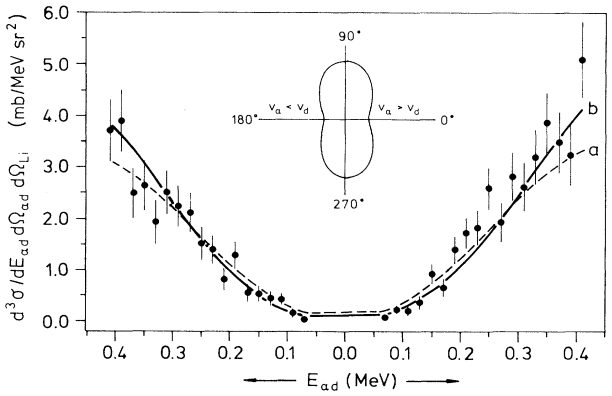

FIG. 10. Comparison of the measured triple-differential cross section of ^{6}Li Coulomb dissociation with various forms of the astrophysical S factor: (a) $S = 1.7 \times 10^{-5}$ MeV mb and (b) $S = (0.91 + 2.92E) \times 10^{-5}$ MeV mb.

gy scale (see discussion of the $^{16}O \rightarrow {}^{12}C + \alpha$ case in Ref. [4]). Such a feature is not observed with our data. Nevertheless, the present simplified analysis, taking only $E2$ excitation into account, and the data at low energies do not exclude non-negligible $E1$ admixtures at energies $E \ll 100$ keV, and the results imply a lower limit of the $d(\alpha,\gamma)^6$Li cross section. More quantitative conclusions need more detailed calculations.

Though different multipole components enter differently the Coulomb dissociation and corresponding capture cross section, we would like to emphasize that the Coulomb dissociation approach provides some useful additional flexibilities. Varying the experimental conditions (the impact parameter b and increasing the virtual photon number by higher projectile energies) may relatively enhance the $E1$ component and help to disentangle various multipoles on the basis of sufficiently precise data. There are also valuable consistency checks.

In order to display the experimental progress due to the application of the Coulomb dissociation approach, the results (with $E \geq 100$ keV) have been converted into cross-section values for the $d(\alpha,\gamma)^6$Li capture reaction and are plotted together with the previous (higher-energy) results of the standard experimental approach (Fig. 11). These results can be considered as an experimental confirmation of theoretical conclusions on the capture cross section at astrophysical energies.

VI. CONCLUSIONS

The nucleosynthesis of the Li isotopes has very interesting aspects [17]. The $d(\alpha,\gamma)^6$Li reaction is considered to be the only mechanism likely to produce ^{6}Li within the big-bang evolution [18]. Based on a theoretical extrapolation of the higher-energy data ($E \geq 1$ MeV) and the resonant transition from the $I = 3^+$ resonance at 0.711 MeV, it was concluded that at the relevant temperature ($T_9 \simeq 1.0$) the capture reaction rate is too low to lead to a significant amount of ^{6}Li during the big bang comparable to the observed abundance and the ^{6}Li/^{7}Li ratio. Hence it is generally believed that ^{6}Li is produced via spallation processes of galactic cosmic rays. Though the present data do not alter these general conclusions, they provide an experimental *ex post* justification. This is not unimportant in view of the theoretical uncertainties and occasional "surprises" with extrapolated cross sections.

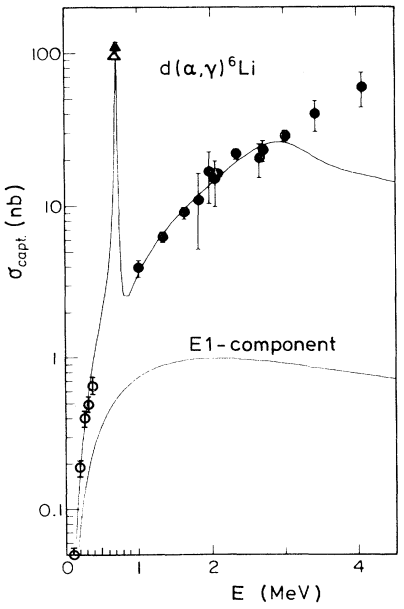

FIG. 11. Cross section for the $d(\alpha,\gamma)^6$Li capture reaction. The low-energy data (open circles) of the present experiment are added to the graph of Ref. [19].

In general, by our investigation projectile breakup in forward-scattering direction is demonstrated to be an access to electromagnetic transition probabilities for low relative energies between the fragments. The approach needs careful study in selecting the angular scattering range where the Coulomb interaction is dominant. The analysis [21] of the sequential breakup data of the present experiments indicates that currently used prescriptions [8,40] for determining the separation of the interacting nuclei are too weak to suppress sufficiently nuclear contributions. Semiclassical trajectory calculations [5,21] prove to be quite helpful to define proper experimental conditions, though quantitative conclusions suffer sometimes from the ambiguities of the nuclear potential, in particular at low projectile energies. Generalizing our observations, the extreme forward angular region, where $\sigma/\sigma_R \approx 1$ appears to be no longer modulated by rainbow effects, is quite safe.

In cases where such conditions are not safely met, spurious nuclear contributions may lead to inconsistencies, even when the Coulomb interaction is dominant. Recently, Hesselbarth *et al.* [41] have experimentally investigated in detail the breakup of the 60 MeV ^{6}Li on ^{208}Pb at scattering angles of 15°, 20°, and 25°. The results show nicely the increasing influence of the nuclear field at larger angles. Conspicuous and peculiar "forward-backward" asymmetries for the nonsequential emission of the breakup fragments from the $\alpha + d$ c.m. system are observed. These larger asymmetries cannot be explained by the Coulomb breakup theory, even admitting an unreasonably large $E1$ admixture. In contrast, the data taken at 156 MeV in the course of the present investigations do show only slight, theoretically consistent asymmetries [42]. This feature additionally supports the pure Coulomb mechanism. We tentatively associate the observation of Hesselbarth *et al.* to the influence of a remaining nuclear field disturbing the angular distribution of fragments of nonresonant dissociation.

There is an interesting proposal [43] of a variant of the Coulomb dissociation approach for situations where nuclear and Coulomb breakup coexist. In order to avoid a detailed decomposition of the nuclear and electromagnetic amplitudes by invoking a reliable theory of nuclear breakup, an *ad hoc* assumption of a "universal" energy dependence of the nuclear and electromagnetic transition strengths is introduced with a standard distorted-wave Born-approximation (DWBA) analysis. This procedure can be criticized as nuclear and electromagnetic form fac-

tors behave asymptotically in a different way and as the nuclear interaction uncertainties are introduced through the DWBA procedure.

The Coulomb dissociation approach is potentially able to give experimental information on the electromagnetic interaction of nuclear particles at extremely low energies (in principle, down to zero energy). With decreasing relative energy of the fragments, dedicated experimental procedures must be used to establish the necessary efficiency and energy resolution. The methods developed in these experiments are of that kind and allow further improvements. It should be emphasized that at the high laboratory energies of the fragments the interaction of *bare* nuclei is involved, in contrast to low-energy capture experiments, which are affected by screening of the atomic electrons [44]. In turn, comparative studies of nuclear fusion at low energies and Coulomb breakup could provide an experimental basis for understanding of the screening problem.

ACKNOWLEDGMENTS

We take the opportunity to thank Prof. Dr. G. Schatz for his encouragement and interest in these studies, and we gratefully acknowledge valuable communications and discussions with Dr. P. Aguer, Dr. J. Hesselbarth, Prof. Dr. K. Langanke, and Dr. D. K. Srivastava. We thank Dipl. Phys. G. Gantenbein for his help in early stages of the measurements. The experiments have benefited from the considerable efforts of the cyclotron operation crew, and of Ing. F. Schulz, in particular, for preparing the ^{6}Li beam with excellent quality.

*Present address: Centre de Spectrométrie Nucléaire et de Spectrométrie de Masse, F-91405 Campus Orsay, France.

[1] H. W. Wittern, Fortschr. Phys. **14**, 401 (1966).
[2] H. A. Weidenmüller and A. Winter, Ann. Phys. (N.Y.) **66**, 218 (1971).
[3] H. Rebel, Kernforschungszentrum Karlsruhe report, 1985 (unpublished); G. Baur, C. A. Bertulani, and H. Rebel, Nucl. Phys. **A458**, 188 (1986).
[4] G. Baur and M. Weber, Nucl. Phys. **A504**, 352 (1989).
[5] D. K. Srivastava and H. Rebel, J. Phys. G **12**, 717 (1986); D. K. Srivastava, D. N. Basu, and H. Rebel, Phys. Rev. C **38**, 2148 (1988).
[6] A. C. Shotter, in *Proceedings of the International Conference on the Nuclear Reaction Mechanism,* Calcutta, 1989, edited by Suprokash Mukherjee (World Scientific, Singapore, 1989), p. 350; A. C. Shotter, J. Phys. G **15**, L41 (1989).
[7] H. Rebel, in *Proceedings of the International Conference on the Nuclear Reaction Mechanism* (Ref. [6]), p. 364.
[8] H. Gemmeke, B. Deluigi, L. Lassen, and D. Scholz, Z. Phys. A **286**, 73 (1978).
[9] C. M. Castaneda, H. A. Smith, Jr., P. P. Singh, and H. Karwowski, Phys. Rev. C **21**, 179 (1980).
[10] T. Shimoda, N. Ikeda, K. Katosi, T. Fukuda, S. Shimoura, T. Mori, T. Komo, and H. Ogata (unpublished).
[11] H. Jelitto, J. Buschmann, V. Corcalciuc, H. J. Gils, N. Heide, J. Kiener, H. Rebel, C. Samanta, and S. Zagromski, Z. Phys. A **332**, 317 (1989).
[12] A. C. Shotter, V. Rapp, T. Davinson, D. Branford, N. E. Sanderson, and M. Nagarajan, Phys. Rev. Lett. **53**, 1539 (1984).
[13] H. Utsunomiya, R. P. Schmitt, Y.-W. Lui, D. R. Haenni, H. Dejbakhsh, L. Cooke, P. Heimberg, A. Ray, T. Tamura, and T. Udagawa, Phys. Lett. B **211**, 24 (1988).
[14] H. Utsunomiya, Y.-W. Lui, L. Cooke, H. Dejbakhsh, D. R. Haenni, P. Heimberg, A. Ray, B. K. Srivastava, and R. P. Schmitt, Nucl. Phys. **A511**, 379 (1990).
[15] D. K. Srivastava, D. N. Basu, and H. Rebel, Phys. Lett. B **206**, 391 (1988).
[16] H. J. Gils, J. Buschmann, S. Zagromski, J. Krisch, and H. Rebel, Nucl. Instrum. Methods A **276**, 151 (1989); H. J. Gils, H. Jelitto, H. Schlösser, S. Zagromski, J. Buschmann, W. Eyrich, A. Hofmann, J. Kiener, A. Lehmann, and H. Rebel, *ibid.* **276**, 169 (1989).
[17] D. N. Schramm, Nature **317**, 386 (1985); D. N. Schramm and R. V. Wagoner, Annu. Rev. Nucl. Sci. **27**, 37 (1977).
[18] Sam M. Austin, Prog. Part. Nucl. Phys. **7**, 1 (1981).
[19] R. G. Robertson, P. Dyer, R. A. Warner, R. C. Melin, T. J. Bowles, A. B. McDonald, G. C. Ball, W. G. Davies, and E. D. Earle, Phys. Rev. Lett. **47**, 1867 (1981).
[20] F. Eigenbrod, Z. Phys. **228**, 337 (1969).
[21] J. Kiener, G. Gsottschneider, H. J. Gils, H. Rebel, V. Corcalciuc, S. K. Basu, G. Baur, and J. Raynal, Z. Phys. A **339**, 489 (1991); R. Shyam, G. Baur, and P. Banerjee, Phys. Rev. C **44**, 915 (1991).
[22] J. Kiener, Kernforschungszentrum Karlsruhe Report No. KfK 4691, 1990.
[23] G. Gantenbein, Kernforschungszentrum Karlsruhe Report No. KfK 4427B, 1988.
[24] H. J. Gils, J. Kiener, S. Zagromski, and H. Rebel, in Kernforschungszentrum Karlsruhe Report No. KfK 4159, 1986, edited by G. Büche, P. Doll, and L. Friedrich, p. 33.
[25] J. Kiener, H. J. Gils, N. Heide, H. Jelitto, H. Rebel, and S. Zagromski, in Kernforschungszentrum Karlsruhe Report No. KfK 4405, 1988, edited by W. Heeringa and F. Voss, p. 43; J. Kiener, H. J. Gils, H. Rebel, G. Baur, G. Gantenbein, N. Heide, H. Jelitto, J. Wentz, and S. Zagromski, in *Heavy Ions in Atomic and Nuclear Physics,* Proceedings of the 20th Mikolajki Summer School on Nuclear Physics, Mikolajki, Poland, 1988, edited by Z. Wilhelmi and G. Szeflinska (Harwood, Chur, 1988), p. 124.
[26] H. Utsunomiya, Y.-W. Lui, and R. P. Schmitt, Nucl. Instrum. Methods A **278**, 744 (1989).
[27] R. Ernst, L. Friedrich, E. Huttel, and F. Schulz, Nucl. Instrum. Methods A **287**, 337 (1990).
[28] G. Gsottschneider, Kernforschungszentrum Karlsruhe Report No. KfK 4803, 1990.
[29] H. J. Gils, Kernforschungszentrum Karlsruhe Report No. KfK 2972, 1980.
[30] J. Kiener, H. J. Gils, N. Heide, H. Jelitto, H. Rebel, J. Wentz, S. Zagromski, D. K. Basu, and I. M. Brâncus, in Kernforschungszentrum Karlsruhe Report No. KfK 4660,

1990, edited by G. Drexlin and H. J. Gils, p. 44.
[31] H. Fuchs, Nucl. Instrum. Methods **200**, 361 (1982).
[32] A. Winther and K. Alder, Nucl. Phys. **A319**, 518 (1979); K. Alder and A. Winther, *Electromagnetic Excitation* (North-Holland, Amsterdam, 1975).
[33] F. Ajzenberg-Selove, Nucl. Phys. **A490**, 38 (1988); R. Yen, L. S. Cardman, D. Kalinsky, H. R. Legg, and C. K. Bockelmann, *ibid.* **A235**, 135 (1978).
[34] M. A. Bernstein and W. A. Friedman, Phys. Rev. C **31**, 843 (1985).
[35] R. Planeta and H. Rebel (unpublished results).
[36] A. Redder, H. W. Becker, C. Rolfs, H. P. Trautvetter, T. R. Donoghue, T. C. Rinckel, J. W. Hammer, and K. Langanke, Nucl. Phys. **A462**, 385 (1987).
[37] K. Langanke and C. Rolfs, Z. Phys. A **325**, 193 (1986).
[38] K. Langanke, Nucl. Phys. **A457**, 351 (1986).
[39] S. Typel, G. Blüge, and K. Langanke, Z. Phys. A **339**, 335 (1991).
[40] R. A. Broglia, *Heavy Ion Reactions,* Vol. 1 of *Lecture Notes* (Benjamin-Cummings, New York, 1981).
[41] J. Hesselbarth, S. Kahn, T. Kihm, and K. T. Knöpfle, Z. Phys. A **331**, 365 (1988); J. Hesselbarth, Ph.D. thesis, University of Heidelberg, 1990.
[42] J. Kiener, H. J. Gils, H. Rebel, and G. Baur, Z. Phys. A **332**, 359 (1989).
[43] H. Utsunomiya, Y. W. Lui, D. R. Haenni, H. Dejbakhsh, L. Cooke, B. K. Srivastava, W. Turmel, D. O'Kelly, R. P. Schmitt, D. Shapira, J. Gomez del'Campo, A. Ray, and T. Udagawa, Phys. Rev. Lett. **65**, 847 (1990).
[44] H. J. Assenbaum, K. Langanke, and C. Rolfs, Z. Phys. A **321**, 461 (1987).